Published in IET Optoelectronics as an invited paper
Received on 18th June 2009
Revised on 12th August 2009
doi: 10.1049/iet-opt.2009.0050

Special Issue – Selected papers inspired by the Semiconductor and Integrated Optoelectronics (SIOE 2009) Conference

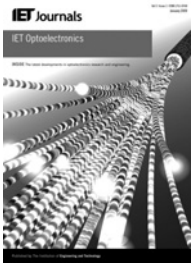

ISSN 1751-8768

Design and characteristics of staggered InGaN quantum-well light-emitting diodes in the green spectral regime

H.P. Zhao[1] *G.Y. Liu*[1] *X.-H. Li*[1] *R.A. Arif*[1] *G.S. Huang*[1]
J.D. Poplawsky[2] *S. Tafon Penn*[2] *V. Dierolf*[2] *N. Tansu*[1]

[1]*Department of Electrical and Computer Engineering, Center for Optical Technologies, Lehigh University, Bethlehem, PA 18015, USA*
[2]*Department of Physics, Center for Optical Technologies, Lehigh University, Bethlehem, PA 18015, USA*
E-mail: Tansu@Lehigh.Edu

Abstract: Staggered InGaN quantum wells (QWs) are investigated both numerically and experimentally as improved active region for light-emitting diodes (LEDs) emitting at 520–525 nm. Based on a self-consistent six-band ***k·p*** method, band structures of both two-layer staggered $In_xGa_{1-x}N/In_yGa_{1-y}N$ QW and three-layer staggered $In_yGa_{1-y}N/In_xGa_{1-x}N/In_yGa_{1-y}N$ QW structures are investigated as active region to enhance the spontaneous emission radiative recombination rate (R_{sp}) for LEDs emitting at 520–525 nm. Numerical analysis shows significant enhancement of R_{sp} for both two-layer and three-layer staggered InGaN QWs as compared to that of the conventional $In_zGa_{1-z}N$ QW. Significant reduction of the radiative carrier lifetime contributes to the enhancement of the radiative efficiency for both two-layer and three-layer staggered InGaN QW LEDs emitting at 520–525 nm. Three-layer staggered InGaN QW LEDs emitting at 520–525 nm was grown by metal-organic chemical vapour deposition (MOCVD) by employing graded-temperature profile. Power density-dependent cathodoluminescence (CL) measurements show the enhancement of peak luminescence by up to 3 times and integrated luminescence by 1.8–2.8 times for the three-layer staggered InGaN QW LED. Electroluminescence (EL) output power of the staggered InGaN QW LED exhibits 2.0–3.5 times enhancement as compared to that of the conventional InGaN QW LED. The experimental results show the good agreement with theory.

1 Introduction

III-Nitride material system as active region for light-emitting diodes (LEDs) and laser diodes (LDs) covers the emission from UV up to visible regime [1–5]. The advances in UV and blue-emitting LEDs based on InGaN quantum-well (QW) active regions have led to relatively high internal quantum efficiency (IQE) [1–3]; however, the extension of emission wavelength by employing InGaN-based QW into green and yellow spectral regimes has been challenging. The AlGaInP material has demonstrated superior device characteristics in the red emission regime [6]. However, the AlGaInP material system has limitation in particular for pushing the emission wavelength down from red spectral regime into yellow spectral regime.

The challenge in the pursuit of high IQE active region for green emission spectral regime is referred as 'green gap' challenge [7]. The InGaN QW LEDs suffer from the low IQE for the green emission, which leads to the significantly lower external quantum efficiency (EQE) for green LEDs [7]. The low IQE in green-emitting InGaN QW active region has also led to challenges in achieving diode lasers emitting in the green regime.

This paper focuses on the InGaN-based QWs as active region for high-performance LEDs emitting at the green regime. The major challenges for high-efficiency green-emitting conventional InGaN QW LEDs include (i) high threading dislocation densities because of the defects generated at the GaN/sapphire interface as well as from

the lattice mismatch between high In-content InGaN QW and the GaN barrier layers; (ii) phase separation in high In-content InGaN QW active region and (iii) significantly reduced electron–hole wavefunction overlap (Γ_{e_hh}) because of the existence of the electrostatic field in the QW.

The strong electrostatic field in InGaN QWs [4] results from both spontaneous polarisation (P_{spon}) and piezoelectric polarisation (P_{piezo}). The P_{spon} in InGaN QWs stems from the non-ideal internal cell parameters (c/a) of the wurtzite III- nitride [0001]-oriented materials. The P_{piezo} in InGaN QWs arises from the lattice mismatch between the InGaN QWs and the GaN barriers, and P_{piezo} is proportional to the lattice mismatch. The existence of the strong electric field from both spontaneous and piezoelectric polarisations causes the charge separation in the InGaN QWs, which leads to a significant reduction of the electron–hole wavefunction overlap (Γ_{e_hh}). Based on Fermi's golden rule, the transition rate between the conduction band and valence band is proportional to the square of the matrix element, which is proportional to the electron–hole wavefunction overlap (Γ_{e_hh}). Thus, the significant reduction of Γ_{e_hh} in InGaN QWs leads to significant reduction in its radiative recombination rate ($\sim|\Gamma_{e\_hh}|^2$).

To extend the emission wavelength for InGaN QW-based LEDs to green and beyond, two approaches can be employed as follows: (i) use higher In-content InGaN QW or (ii) employ InGaN QW with larger QW thickness. However, both approaches lead to severe reduction of electron–hole wavefunction overlap (Γ_{e_hh}). Hence, in order to enhance the efficiency for InGaN QW-based LEDs emitting at the green regime, improvement of the electron–hole wavefunction overlap (Γ_{e_hh}) is very important.

Recently, several approaches have been proposed to enhance the electron–hole wavefunction overlap (Γ_{e_hh}) such as (i) the use of non-polar InGaN QW [8], (ii) the use of InGaN QW with δ-AlGaN layer [9, 10], (iii) staggered InGaN QW [11–16], (iv) type-II InGaN–GaNAs QW [17, 18] and (v) strain-compensated InGaN–AlGaN QW [19, 20]. In the approach for non-polar InGaN QW LEDs [8], the growths of the QWs were conducted on m-plane or a-plane GaN template. The approaches in [9–20] focus on the pursuit of nitride QWs grown on c-plane GaN templates. All these approaches [8–20] focused on increasing the radiative recombination rate of the InGaN-based QW by improving the electron–hole wavefunction overlap (Γ_{e_hh}) in the QW.

Previously, the two-layer staggered InGaN QW employing step-function like In-content in the QW had been implemented into LED device structure for emission in the blue spectral regime [11, 12]. The use of two-layer staggered InGaN QW LEDs led to improvement in output power and efficiency of the devices.

In this paper, we present both numerically and experimentally the optimisation studies of the staggered InGaN QW by engineering the In-content and sub-layer thickness of the staggered InGaN QWs emitting at 520–525 nm. Based on a self-consistent six-band $\boldsymbol{k\cdot p}$ model for wurtzite semiconductor, both the electron–hole wavefunction overlap (Γ_{e_hh}) and spontaneous emission radiative recombination rate (R_{sp}) of the optimised two-layer staggered $In_{33}Ga_{0.67}N$ ($d_{W1} = 1.8$ nm)/$In_{0.17}Ga_{0.83}N$ QW ($d_{W2} = 1.2$ nm) structure and three-layer staggered $In_{0.17}Ga_{0.83}N$ ($d_{W1} = 0.6$ nm)/$In_{0.33}Ga_{0.67}N$ ($d_{W2} = 1.8$ nm)/$In_{0.17}Ga_{0.83}N$ ($d_{W3} = 0.6$ nm) QW structure are investigated and compared to that of the conventional $In_{0.28}Ga_{0.72}N$ ($d_{QW} = 3$ nm) QW. Experimentally, three-layer staggered InGaN QW LED was grown by metalorganic chemical vapour deposition (MOCVD) employing graded temperature profile. Power density-dependent cathodoluminescence (CL) measurement was conducted for the three-layer staggered InGaN QW LED as compared to that of the conventional InGaN QW LED, which indicated a significant enhancement of CL at different injected electron power density. Electroluminescence (EL) comparison for the three-layer staggered InGaN QW LED and the conventional InGaN QW LED shows enhanced performance of the three-layer staggered InGaN QW LED.

The organisation of this paper is presented as follows. Section 2 introduces the concept of two-layer staggered $In_xGa_{1-x}N/In_yGa_{1-y}N$ QW and three-layer staggered $In_yGa_{1-y}N/In_xGa_{1-x}N/In_yGa_{1-y}N$ QW structures. In Section 3, the theoretical and numerical formulation is presented briefly. The spontaneous emission radiative recombination rate (R_{sp}) is discussed for staggered InGaN QWs emitting at 520–525 nm in Section 4. The radiative carrier lifetime and radiative efficiency of staggered InGaN QWs LEDs are discussed in Section 5, and the results will be compared with those of conventional InGaN QW LEDs. Section 6 discusses the effect of the Auger recombination on the radiative efficiency on both conventional and staggered InGaN QWs. In Section 7, the MOCVD growth of three-layer staggered InGaN QW LED employing temperature profile will be presented followed by the power density-dependent CL measurement and EL characterisation for three-layer staggered InGaN QW LED as compared to that of the conventional InGaN QW LED in Section 8.

2 Concepts of staggered InGaN QWs

The existence of electrostatic field in the InGaN QW results in 'charge separation' effect in the QW, which leads to spatial separations of the electrons and holes in the QW. The charge separation in conventional InGaN QW leads to a severe reduction of the electron–hole wavefunction overlap (Γ_{e_hh}), in comparison to that of non-polar QW structure. The low electron–hole wavefunction overlap (Γ_{e_hh}) in

IET Optoelectron., 2009, Vol. 3, Iss. 6, pp. 283–295
doi: 10.1049/iet-opt.2009.0050

conventional InGaN QWs active region leads to significant reduction in radiative recombination and low radiative efficiency for nitride LEDs, in particular as the emission wavelength is extended to green spectral regime. The purpose of employing the staggered InGaN QW design is to enhance the electron–hole wavefunction overlap (Γ_{e_hh}) by engineering the band lineups of the InGaN QW, hence leading to increase in the radiative recombination rate (R_{sp}) and radiative efficiency of the QW for LEDs application.

In this paper, three QW structures are studied and compared as follows: (a) the conventional $In_zGa_{1-z}N$ QW; (b) the two-layer staggered $In_xGa_{1-x}N/In_yGa_{1-y}N$ QW and (c) the three-layer staggered $In_yGa_{1-y}N/In_xGa_{1-x}N/In_yGa_{1-y}N$ QW structures, which are surrounded by GaN barrier layers. Note that the three structures have the same total QW thickness (d_{QW}) for comparison purpose. The conventional $In_zGa_{1-z}N$ QW contains uniform In-content (z) with the QW thickness of d_{QW}. The two-layer staggered $In_xGa_{1-x}N/In_yGa_{1-y}N$ QW is characterised by the use of a step-function like In-content profile in the QW as follows: (i) high In-content of x with thickness of d_{w1} and (ii) lower In-content of y with thickness of d_{w2}, where $d_{w1} + d_{w2} = d_{QW}$. In contrast to the two-layer staggered InGaN QW, the three-layer staggered $In_yGa_{1-y}N/In_xGa_{1-x}N/In_yGa_{1-y}N$ QW contains the higher In-content (x) sub-layer in the centre, which is sandwiched between two InGaN sub-layers with lower In-content of y. The total thickness (d_{QW}) of the three-layer staggered InGaN QW is also designed as equal to $d_{QW} = d_{w1} + d_{w2} + d_{w3}$. To compare the performance of the active regions of these three structures for LED application, the In-contents and sub-layer thickness for the conventional InGaN QW, two-layer staggered $In_xGa_{1-x}N/In_yGa_{1-y}N$ QW and three-layer staggered $In_yGa_{1-y}N/In_xGa_{1-x}N/In_yGa_{1-y}N$ QW are designed such that all three QWs emit at similar peak emission wavelength.

By engineering the energy band lineups, the electron–hole wavefunction overlap (Γ_{e_hh}) of the staggered InGaN QWs can be significantly enhanced. The concept of two-layer staggered InGaN QW was proposed in [11, 12]. The concept of three-layer staggered InGaN QW for LED application was proposed and experimentally studied in [13, 14], respectively. Thus, both the two-layer and three-layer staggered InGaN QWs are expected to have higher spontaneous emission radiative recombination rate (R_{sp}) than that of the conventional InGaN QW, which in turn leads to enhancement in radiative and IQE of the LEDs.

3 Theoretical and numerical formulation

The band structure calculation for the conventional and staggered InGaN QWs is based on self-consistent six-band $\boldsymbol{k\cdot p}$ formalism for wurtzite semiconductors [20–23]. The calculation takes into account the valence band mixing, the strain effect and the spontaneous and piezoelectric polarisations as well as the carrier screening effect. To take into consideration the carrier screening effect, the confined eigen-energies and corresponding wavefunction are calculated self-consistently via the Schrödinger and Poisson equations [20, 23]. Note that the six-band $\boldsymbol{k\cdot p}$ method considers the band mixing and coupling within the valence band. In this calculation, the band structure for the conduction band uses parabolic approximation. The coupling between the conduction band and valence band is negligible for the case of the wide bandgap InGaN material system [21, 22].

For the QW structures, the momentum matrix elements ($|M_{sp}|^2$) become polarisation dependent including both TE polarisation ($|M_{TE}|^2$) and TM polarisation ($|M_{TM}|^2$) terms. In this study, the spontaneous emission rate is obtained by averaging of the momentum matrix elements of three polarisations as $|M_{sp}|^2 = (2|M_{TE}|^2 + |M_{TM}|^2)/3$. The details of the self-consistent numerical formulation for InGaN-based QW active regions employing self-consistent six-band $\boldsymbol{k\cdot p}$ formalism are presented in [20].

The material parameters of binary InN, GaN for the band structure calculation are obtained from [24, 25], which are summarised in the table in [20]. The parameters for the ternary alloy InGaN are obtained by linear interpolation of that of the binary InN and GaN, except for the energy gap of InGaN. The bandgap for $In_xGa_{1-x}N$ is obtained as follows: $E_g(In_xGa_{1-x}N) = xE_g(InN) + (1-x)E_g(GaN) - bx(1-x)$, where the bowing parameter (b) is 1.4 eV [24]. The band offset ratio (ΔE_c:ΔE_v) of InGaN/GaN is assumed to be 0.7:0.3 [26].

The finite difference approach is employed to solve the Schrodinger's and Poisson's equations for semiconductor heterostructure or nanostructure [20, 27]. The discretised step size is 1 Å. The thickness of the GaN barriers is assumed to be much thicker than the InGaN QW, which ensures the evanescence of the envelope wavefunction in the GaN barriers for both conduction band and valence band. The potential band lineups are solved self-consistently based on the Poisson's equation [23]. The convergence condition is set such as the tolerance of the eigen-energy is less than 0.1%.

4 Spontaneous emission radiative recombination for staggered InGaN QWs

Fig. 1 shows the energy band lineup profiles and the wavefunction of the first conduction subband (C1) and the first valence subband (HH1) at zone centre for (a) conventional 30-Å $In_{0.28}Ga_{0.72}N$ QW, (b) two-layer staggered 18-Å $In_{0.33}Ga_{0.67}N$/12-Å $In_{0.17}Ga_{0.83}N$ QW and (c) three-layer staggered 6-Å $In_{0.17}Ga_{0.83}N$/18-Å $In_{0.33}Ga_{0.67}N$/6 - Å $In_{0.17}Ga_{0.83}N$ QW. The structures are

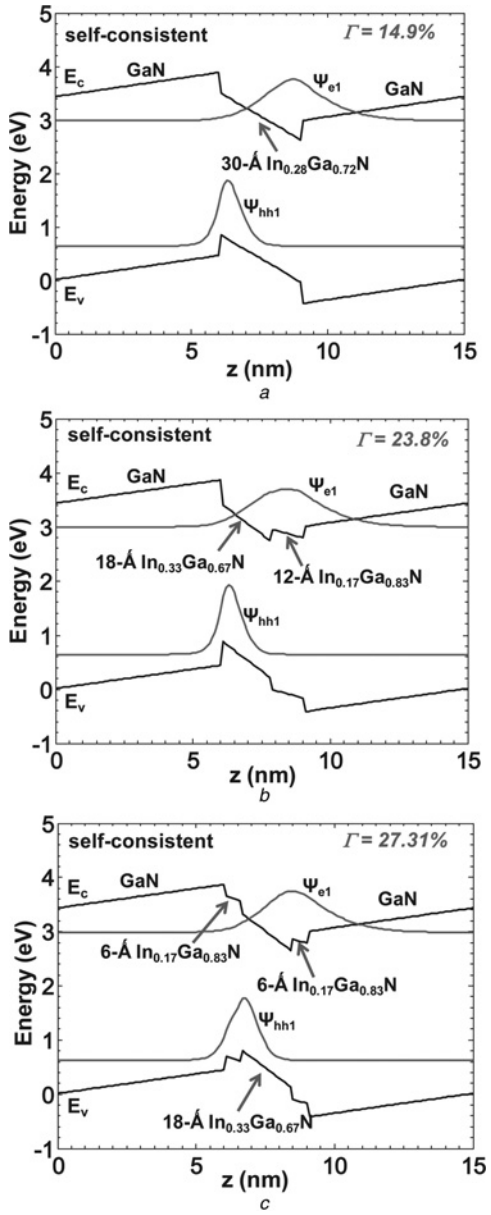

Figure 1 *Energy band lineups*

a Conventional 30-Å $In_{0.28}Ga_{0.72}N$ QW
b Two-layer staggered 18-Å $In_{0.33}Ga_{0.67}N$/12-Å $In_{0.17}Ga_{0.83}N$ QW
c Three-layer staggered 6-Å $In_{0.17}Ga_{0.83}N$/18-Å $In_{0.33}Ga_{0.67}N$/6-Å $In_{0.17}Ga_{0.83}N$ QW
All three QW structures are designed for $\lambda \sim 520-525$ nm

specifically designed such that all three QWs emit at ~520–525 nm. As shown in Fig. 1*a*, a large spatial separation between electron and hole wavefunction is observed in the conventional InGaN QW because of the existence of the strong internal electric field and with the electron–hole wavefunction overlap (Γ_{e_hh}) of 14.9%. Fig. 1*b* shows the two-layer staggered InGaN QW design employing a step-function like In-content for the QW, and the use of these two-layer design leads to the electron wavefunction being pushed to the centre of the QW resulting in enhanced electron–hole wavefunction overlap (Γ_{e_hh}) of 23.8%. Fig. 1*c* shows three-layer staggered InGaN QW with higher In-content sub-layer in the centre sandwiched between two sub-layers with lower In-content. In the three-layer QW, both the electron and hole wavefunctions are pushed to the centre of the QW resulting in increase in the electron–hole wavefunction overlap (Γ_{e_hh}) of 27.31%. By optimising the In-contents and thicknesses of the sub-layers for both two-layer staggered InGaN QW and three-layer staggered InGaN QW, the electron–hole wavefunction overlap (Γ_{e_hh}) of the staggered InGaN QW is improved by 1.6–1.8 times with similar emission wavelength of 520–525 nm.

Fig. 2 shows the calculated spontaneous emission spectra for conventional InGaN QW (dash-dot line), two-layer staggered InGaN QW (dash line) and three-layer staggered InGaN QW (solid line) at carrier densities (N) of $N = 2 - 10 \times 10^{18}$ cm^{-3} at $T = 300$ K. The spontaneous emission rate is obtained by taking into account all possible transitions between nth conduction subbands and mth valence subbands as follows

$$r^{\text{spon}}(\hbar\omega) = \frac{2q^2\pi}{n_r c\varepsilon_0 m_0^2 \omega L_\omega} \sum_{\sigma=U,L} \sum_{n,m} \int \frac{k_t \mathrm{d}k_t}{2\pi} |(M)_{nm}(k_t)|^2 \times \frac{f_n^{\text{c}}(k_t)(1 - f_{\sigma m}^{\text{v}}(k_t))(\gamma/\pi)}{(E_{\sigma,nm}^{\text{cv}}(k_t) - \hbar\omega)^2 + \gamma^2} \quad (1)$$

where $f_n^{\text{c}}(k_t)$ and $f_{\sigma m}^{\text{v}}(k_t)$ are the Fermi–Dirac distribution functions for the electrons in conduction band and valence band, and k_t is the in-plane wavevector, L_w is the thickness of the QW, $(M)_{nm}(k_t)$ is the momentum matrix element between nth conduction subband and mth valence subband. Owing to the asymmetry of the band lineups for the conduction band and valence band, the transitions between states with unequal quantum numbers ($m \neq n$) are non-zero. In this calculation, all possible transitions between the

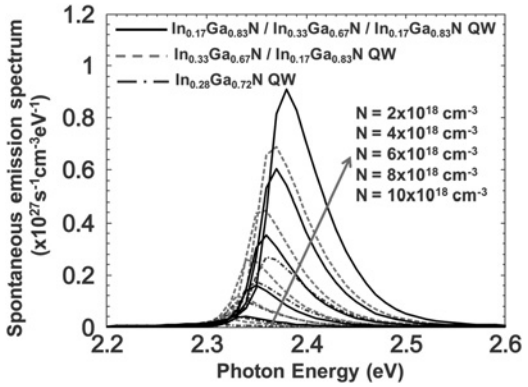

Figure 2 *Spontaneous emission spectra for conventional 30-Å $In_{0.28}Ga_{0.72}N$ QW, two-layer staggered 18-Å $In_{0.33}Ga_{0.67}N$/12-Å $In_{0.17}Ga_{0.83}N$ QW and three-layer staggered 6-Å $In_{0.17}Ga_{0.83}N$/18-Å $In_{0.33}Ga_{0.67}N$/6-Å $In_{0.17}Ga_{0.83}N$ QW emitting at ~520–525 nm for increasing carrier density $N = 2-10 \times 10^{18}$ cm^{-3}*

doi: 10.1049/iet-opt.2009.0050

confined states of the conduction bands and valence bands are taken into account.

From Fig. 2, the spontaneous emission spectra for staggered InGaN QWs are significantly enhanced as compared to that of the conventional InGaN QW for each carrier density. For the case of $N = 10 \times 10^{18}$ cm^{-3}, the two-layer staggered InGaN QW shows approximately 2.56 times higher of the peak spontaneous emission spectra (0.688×10^{27} s^{-1} cm^{-3} eV^{-1}) than that of the conventional one (0.268×10^{27} s^{-1} cm^{-3} eV^{-1}). The three-layer staggered InGaN QW (0.91×10^{27} s^{-1} cm^{-3} eV^{-1}) shows 3.4 times higher than that of the conventional InGaN QW. Note that the peaks of the spontaneous emission spectra for both the conventional InGaN QW and staggered InGaN QWs show blue-shift as the carrier density increases.

The total spontaneous emission radiative recombination rate per unit volume (s^{-1} cm^{-3}) is obtained by integrating (1) over the entire frequency range as follows

$$R_{sp} = \int_0^{\infty} r^{spon}(\hbar\omega)\, d(\hbar\omega) \tag{2}$$

Fig. 3 illustrates the spontaneous emission radiative recombination rate per unit volume (R_{sp}) for the conventional InGaN QW, the two-layer staggered InGaN QW and the three-layer staggered InGaN QW as a function of the carrier density up to 10×10^{18} cm^{-3}. For the two-layer staggered InGaN QW, the enhancement of the spontaneous emission radiative recombination rate (R_{sp}) ranges between 1.82 and 2.74 times at each carrier density as compared to the conventional InGaN QW. The enhancement of the R_{sp} for the three-layer staggered InGaN QW as compared to the conventional InGaN QW ranges between 2.03 and 3.78 times.

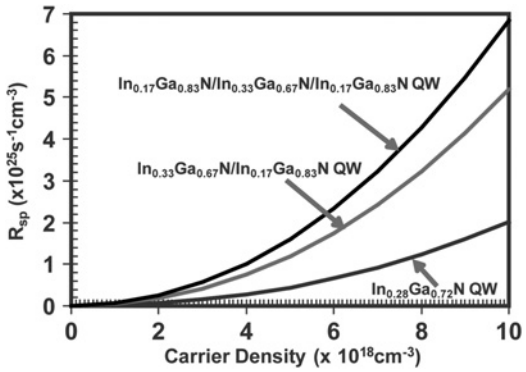

Figure 3 *Spontaneous emission radiative recombination rate (R_{sp}) as a function of carrier density for conventional 30-Å $In_{0.28}Ga_{0.72}N$ QW, two-layer staggered 18-Å $In_{0.33}Ga_{0.67}N$/12-Å $In_{0.17}Ga_{0.83}N$ QW and three-layer staggered 6-Å $In_{0.17}Ga_{0.83}N$/18-Å $In_{0.33}Ga_{0.67}N$/6-Å $In_{0.17}Ga_{0.83}N$ QW at room temperature*

5 Carrier lifetime and radiative efficiency for staggered InGaN QWs

The radiative efficiency (η_{Rad}) is defined as the ratio of recombination current in the QW that recombines radiatively resulting in photon generation as following

$$\eta_{Rad} = \frac{R_{sp}}{R_{non\_rad} + R_{sp}} \tag{3}$$

where the non-radiative recombination rate R_{non_rad} consists of both the monomolecular and Auger recombination rates in the QW as follows

$$R_{non\_rad} = AN + CN^3 \tag{4}$$

Owing to the negligible value of the Auger coefficient in the InGaN-based wide bandgap material system [28, 29], the non-radiative part only take into account the monomolecular recombination in this analysis. Thus, the radiative efficiency of InGaN QW LEDs can be expressed as

$$\eta_{Rad} = \frac{R_{sp}}{AN + R_{sp}} \tag{5}$$

Further discussion on the impacts of Auger recombination on the radiative efficiency of InGaN QW LEDs will be discussed in Section 6.

The total carrier lifetime (τ_{total}) composes of both the radiative lifetime (τ_{rad}) and non-radiative lifetime (τ_{non_rad}), as follows

$$\frac{1}{\tau_{total}} = \frac{1}{\tau_{rad}} + \frac{1}{\tau_{non\_rad}} \tag{6}$$

where

$$\frac{1}{\tau_{Rad}} = \frac{R_{sp}}{N} \tag{7}$$

$$\frac{1}{\tau_{non\_rad}} = \frac{R_{non\_rad}}{N} \tag{8}$$

$$\frac{1}{\tau_{total}} = \frac{R_{sp} + R_{non\_rad}}{N} \tag{9}$$

The relation of the radiative current density and radiative recombination rate is related by the following equation

$$J_{rad} = qd_{QW}R_{sp} \tag{10}$$

Fig. 4*a* compares the radiative lifetime (τ_{rad}) for the conventional InGaN QW, two-layer staggered InGaN QW and three-layer staggered InGaN QW as a function of the carrier density up to 50×10^{18} cm^{-3} for the QW structures discussed in Section 4. The radiative carrier lifetime (τ_{rad}) of the staggered InGaN QWs is reduced because of the

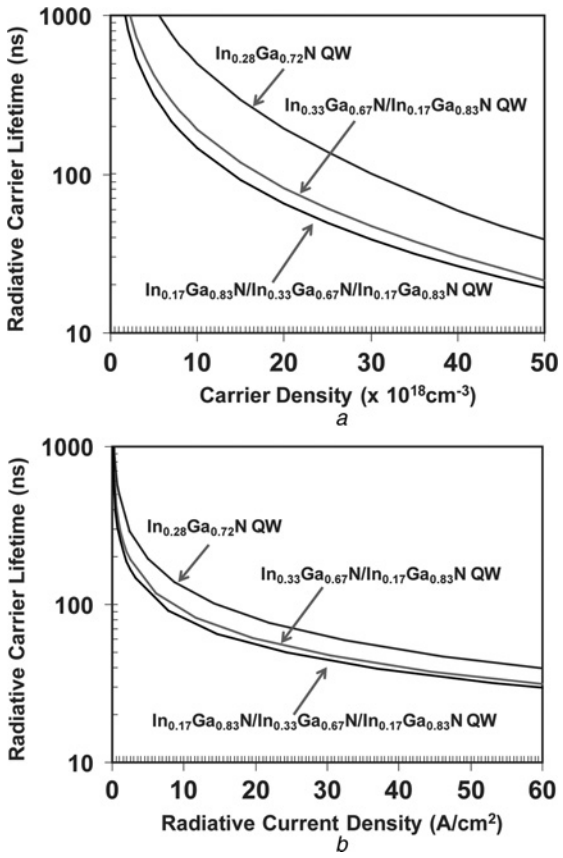

Figure 4 *Radiative lifetime for conventional 30-Å $In_{0.28}Ga_{0.72}N$ QW, two-layer staggered 18-Å $In_{0.33}Ga_{0.67}N$/12-Å $In_{0.17}Ga_{0.83}N$ QW and three-layer staggered 6-Å $In_{0.17}Ga_{0.83}N$/18-Å $In_{0.33}Ga_{0.67}N$/6-Å $In_{0.17}Ga_{0.83}N$ QW emitting at ~520–525 nm as a function of*

a The carrier density up to 50×10^{18} cm^{-3}
b The radiative current density

improved spontaneous emission radiative recombination rate (R_{sp}) as compared to that of the conventional InGaN QW. From Fig. 4*a*, the radiative carrier lifetime (τ_{rad}) of the two-layer staggered InGaN QW is reduced by 45.1–63.5% as compared to that of the conventional InGaN QW at different carrier density, whereas the radiative carrier lifetime (τ_{rad}) of the three-layer staggered InGaN QW is reduced by 50.9–73.5% ($\lambda \sim 520$–525 nm).

To better understand the relationship between the carrier lifetime and the current density, Fig. 4*b* shows the radiative carrier lifetime (τ_{rad}) against the radiative current density for the conventional, two-layer staggered, and three-layer staggered InGaN QWs emitting at 520–525 nm. Fig. 4*b* shows similar trend as that of Fig. 4*a*, which indicates that the radiative carrier lifetimes for staggered InGaN QWs (both two-layer and three-layer staggered InGaN QWs) structures significantly reduce, in comparison to that of the conventional InGaN QW for the radiative current density analysed up to 60 A/cm^2. Note that the longer radiative lifetimes observed for InGaN QWs emitting in the 520–525 nm is a result of the lower optical matrix element in these QWs, in comparison to those observed for blue-emitting InGaN QWs active regions.

The total carrier lifetime (τ_{total}) can be obtained from (9). Note that in the current analysis, we have only taken into account the monomolecular recombination process for the non-radiative recombination. The monomolecular recombination coefficient (A) have been widely reported from the range of $A = 1 \times 10^7$ s^{-1} up to $A = 3 \times 10^8$ s^{-1} [30–32], and these discrepancies on the reported values can be attributed to the varying material quality reported by different groups. As our goal is to investigate the limitation presented by relatively high-quality InGaN QW with low dislocation density, we employed the experimentally reported monomolecular recombination coefficient $A = 3 \times 10^7$ s^{-1} similar to the experiment results reported in [30]. Further discussion on the impacts of Auger recombination in InGaN QW will be discussed separately in Section 6.

The total carrier recombination lifetimes as functions of carrier density in the QWs are plotted in Fig. 5*a* for QWs

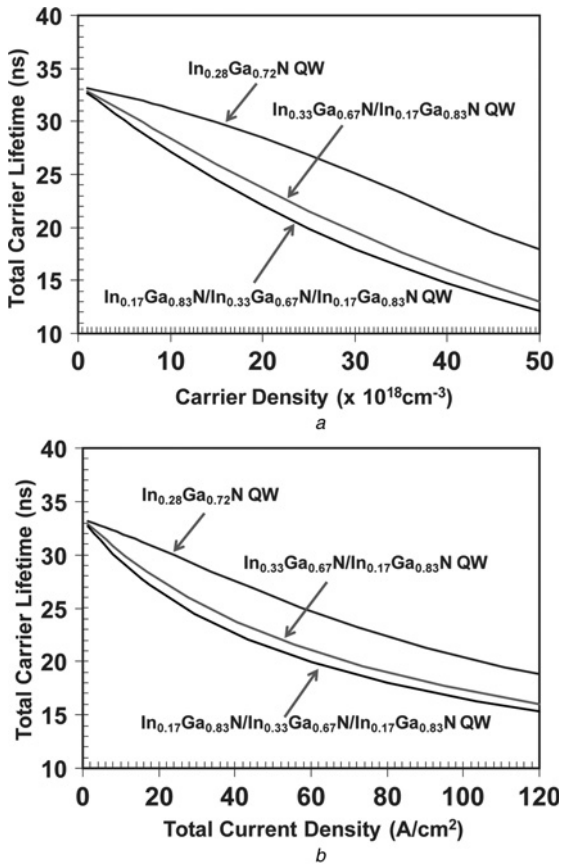

Figure 5 *Total carrier lifetimes for conventional 30-Å $In_{0.28}Ga_{0.72}N$ QW, two-layer staggered 18-Å $In_{0.33}Ga_{0.67}N$/12-Å $In_{0.17}Ga_{0.83}N$ QW and three-layer staggered 6-Å $In_{0.17}Ga_{0.83}N$/18-Å $In_{0.33}Ga_{0.67}N$/6-Å $In_{0.17}Ga_{0.83}N$ QW emitting at ~520–525 nm as a function of*

a The carrier density up to 50×10^{18} cm^{-3}
b The total current density

doi: 10.1049/iet-opt.2009.0050

emitting in the 520–525 nm. It is interesting to note that significant reduction in the total carrier lifetimes were observed because of the use of staggered InGaN QWs. The use of three-layer staggered InGaN QW leads to the most optimised QW structures with lowest carrier lifetimes. Note that all the QWs studied here assumed similar monomolecular recombination coefficient (A). The use of low A value is realistic in particular for high-quality InGaN QW material, and the reported carrier lifetimes here are comparable with the total carrier lifetimes reported from experiments [32, 33]. Fig. 5*b* shows the total carrier lifetime against the total current density for conventional, two-layer staggered and three-layer staggered InGaN QWs. Fig. 5*b* indicates that the total carrier lifetime decreases for both two-layer and three-layer staggered InGaN QWs as compared to that of the conventional InGaN QW for both structures emitting at 520–525 nm.

Based on (3)–(5), the radiative efficiency (η_{Rad}) as a function of carrier density (N) (Fig. 6*a*) and total current density (Fig. 6*b*) in QW is calculated for the conventional InGaN QW, two-layer staggered InGaN QW and three-layer staggered InGaN QW for the structures discussed in Section 4. In Fig. 6*a*, the carrier density in the QW was calculated up to 50×10^{18} cm^{-3}. Note that the radiative efficiency (η_{Rad}) increases as the carrier density increases, because of the stronger carrier dependency of the radiative recombination rate (R_{sp}). Both Figs. 6*a* and *b* show the similar trend. The radiative efficiency (η_{Rad}) is enhanced by 1.32–2.32 times and 1.38–3.72 times for the two-layer staggered InGaN QW and three-layer staggered InGaN QW as compared to that of the conventional InGaN QW. In the low carrier density/current density regime, the conventional InGaN QWs exhibited relatively low radiative efficiency, whereas both the staggered InGaN QW designs exhibited significantly higher radiative efficiency. Only at very high carrier density/current density level, the radiative recombination rate in the conventional InGaN QW design increases. However, it is important to note that high carrier density/current density operation may not be favourable for optimised InGaN QW LED device operation; in particular, thermionic carrier leakage may limit the current injection efficiency in QW LEDs or lasers devices [34].

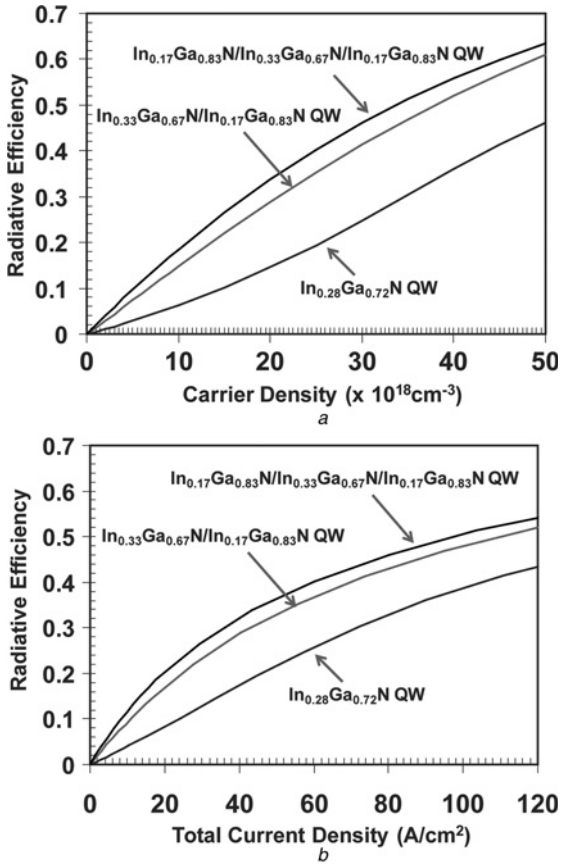

Figure 6 *Radiative efficiency conventional 30-Å $In_{0.28}Ga_{0.72}N$ QW, two-layer staggered 18-Å $In_{0.33}Ga_{0.67}N$/12-Å $In_{0.17}Ga_{0.83}N$ QW and three-layer staggered 6-Å $In_{0.17}Ga_{0.83}N$/18-Å $In_{0.33}Ga_{0.67}N$/6-Å $In_{0.17}Ga_{0.83}N$ QW emitting at ~520–525 nm as a function of*

a The carrier density up to 50×10^{18} cm^{-3}
b The total current density

By utilising both of the two-layer and three-layer staggered InGaN QW structures, the electron–hole wavefunction overlap (Γ_{e_hh}) is greatly enhanced especially when one extends the emission wavelength to green spectral regime and longer. The improved electron–hole wavefunction overlap (Γ_{e_hh}) leads to the enhancement of the spontaneous emission radiative recombination rate (R_{sp}) for the staggered InGaN QWs, which results in the reduced radiative carrier lifetime (τ_{rad}) and improved radiative efficiency (η_{Rad}). Note that the analysis presented here did not take into account many-body Coulomb effects [35]. Recent simulations of two-layer staggered InGaN QWs by Park *et al.* [15] have taken into account the many-body effects and have shown trends that are similar to our results [13].

Note that the radiative efficiency presented in both Figs. 6*a* and *b* did not take into account the contribution of current injection efficiency in the InGaN QW LEDs. It is important to note that the internal efficiency in the III-nitride LEDs depends on both the contribution from the current injection efficiency and radiative efficiency of InGaN QW active region. The discussion of the current injection efficiency for InGaN QW LEDs is beyond the scope of this paper. The current injection efficiency of QW LEDs and lasers depends strongly on the interplay of carrier capture and thermionic emission of carriers in QW–barrier heterostructures, carrier transports, and carrier recombinations in QW and barrier regions [34].

6 Impacts of Auger recombination on radiative efficiency of InGaN QW LEDs

The Auger recombination rate in wide bandgap III-nitride semiconductor is predicted to be significantly lower, in

comparison to that of monomolecular and radiative recombination rates. Recent theoretical studies predicted Auger recombination coefficients in the range of $C = 3.5 \times 10^{-34}$ cm^6/s [28] up to $C = 0.9–1 \times 10^{-32}$ cm^6/s [29]. However, it is important to note that recent experimental studies have indicated the possibility that the Auger recombination coefficient in thick InGaN/GaN double heterostructure active regions ($d_{Active} = 10–77$ nm) in the range of $C = 1.4 \times 10^{-30}$ cm^6/s up to $C = 2 \times 10^{-30}$ cm^6/s [30]. Further studies are still required to clarify and confirm the Auger coefficients (C_{Auger}) for InGaN/GaN QW system, because of the large discrepancies from the reported Auger coefficients in [28–30].

In the radiative efficiency studies presented in Section 5, we specifically did not take into account Auger processes in the analysis. However, in this section, we will present the radiative efficiency analysis of the staggered InGaN QW by taking into account both the upper limit and lower limit of the reported Auger coefficients.

Fig. 7 shows the radiative efficiency of the 520–525 nm emitting InGaN QW active regions for various designs by taking into account $C = 2 \times 10^{-33}$ cm^6/s (lower limit) up to $C = 2 \times 10^{-31}$ cm^6/s (upper limit). These upper and lower limits of the Auger coefficients were used to represent the large range of values reported in [28–30]. As the analysis presented in Fig. 7 is intended to illustrate the trend in the radiative efficiency characteristics of staggered InGaN QWs by taking into account the Auger recombination process, we provide the comparison studies for the optimised three-layer staggered InGaN QW and conventional InGaN QW. The inclusion of the lower limit Auger coefficient modifies the radiative efficiency relation very slightly, and the radiative efficiency relation appears to be relatively similar to

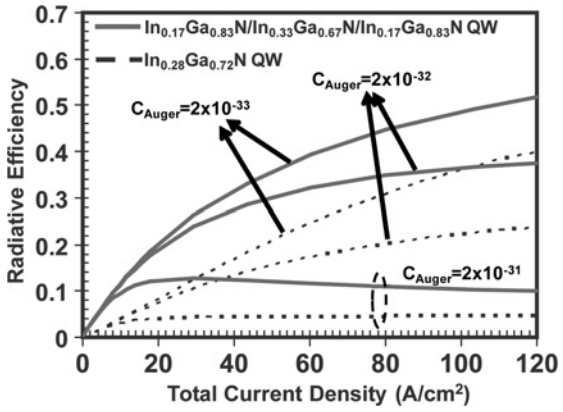

Figure 7 *Radiative efficiency for conventional 30-Å $In_{0.28}Ga_{0.72}N$ QW and three-layer staggered 6-Å $In_{0.17}Ga_{0.83}N$/18-Å $In_{0.33}Ga_{0.67}N$/6-Å $In_{0.17}Ga_{0.83}N$ QW emitting at ~520–525 nm as a function of the total current density*

The analyses take into account Auger coefficient from $C = 2 \times 10^{-33}$ cm^6/s (lower limit) up to $C = 2 \times 10^{-31}$ cm^6/s (upper limit)

that computed in Fig. 6*b*. However, for the case of upper limit Auger coefficient, the significantly larger Auger recombination rate results in relatively low radiative efficiency at high current injection level. The use of staggered InGaN QW results in improvement in radiative efficiency for all Auger coefficients considered here.

Our analysis indicated that the use of staggered InGaN QW active regions with enhanced radiative recombination rate is significantly more important, in the event that Auger recombination coefficient is large in InGaN QW. The Auger process follows $\sim N^3$ relation, thus the non-radiative processes will be dominant as the carrier density in the QW increases.

7 MOCVD growth of staggered InGaN QW LEDs

Based on the numerical simulation and analysis presented in previous sections, both two-layer and three-layer staggered InGaN QWs exhibited significant increase in radiative recombination rate in comparison to that of conventional InGaN QW. The three-layer staggered InGaN QW structure shows optimised spontaneous emission radiative recombination rate and radiative efficiency, in comparison to those of conventional and two-layered staggered InGaN QW active regions.

In this section, we present the growths of three-layer staggered InGaN QW LEDs emitting in the 520–525 nm spectral regime employing graded temperature profile, with the QW structure designed specifically for improved electron–hole wave-function overlap to enhance the radiative recombination rate and radiative efficiency of LED device. Previously, the two-layer staggered InGaN QW [11, 12] with step-function like In-content was used to enhance the electron–hole wavefunction overlap leading to improved radiative efficiency and output power of blue-emitting LED devices, and the compositional engineering of the In-contents was accomplished by modifying the In-precursor (TMIn) flow rate into the chamber during the InGaN QW growth. In our current studies, the green-emitting three-layer staggered InGaN QW was grown by MOCVD with graded temperature profile, as shown in Fig. 8. The use of graded temperature profile during the growth leads to more practical and repeatable approach to grow staggered InGaN QW. To grow high In-content InGaN QW is challenging because of the weak bond strength of InN; as a consequence, the incorporation of indium into the InGaN layer is very sensitive to the growth temperature. As shown in Fig. 8, the three-layer staggered $In_yGa_{1-y}N/In_xGa_{1-x}N/In_yGa_{1-y}N$ QW is composed of three layers (layer #1, layer #2 and layer #3). The growth condition for the three-layer staggered InGaN QW is designed as follows: layer #1 is grown at T_1 (°C) for t_1 (s), layer #2 is grown at T_2 (°C) for t_2 (s) and layer #3 is grown at T_1 (°C) for t_1 (s). Between layer #1 and layer #2, the

doi: 10.1049/iet-opt.2009.0050

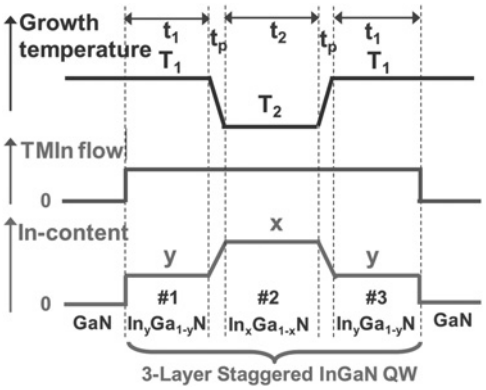

Figure 8 *Schematics of the growth temperature, TMIn-flow rate and In-content for the growths of three-layer staggered InGaN QW with graded temperature profile*

temperature is ramped up from T_1 to T_2 by t_p (s). Similarly, between layer #2 and layer #3, the temperature is ramped down from T_2 to T_1 by t_p (s). Note that constant TMIn, TMGa and NH_3 flow rates are used during the three-layer staggered InGaN QW growth. The real growth temperature profile contains brief overshoot during the ramp-up and ramp-down layer growths. By utilising the graded temperature profile, the composition of In-content in InGaN layer can be engineered to form three-layer staggered InGaN QW structure.

Fig. 9 shows the calibration studies on the In-content incorporated into the MOCVD-grown $In_xGa_{1-x}N$ layer as a function of the growth temperature. All the samples for the calibration studies of the In-content were grown on 2.5-μm thick undoped GaN template on *c*-plane sapphire substrates. The growth of InGaN layer employs TMIn, TEGa and NH_3 as the precursors, and N_2 gas was employed as carrier gas. The V/III and [TMIn]/[Group III] molar ratios were kept constant at 10 200 and 0.38, respectively. By changing the growth temperature, various In-contents in the InGaN layer can be obtained. The

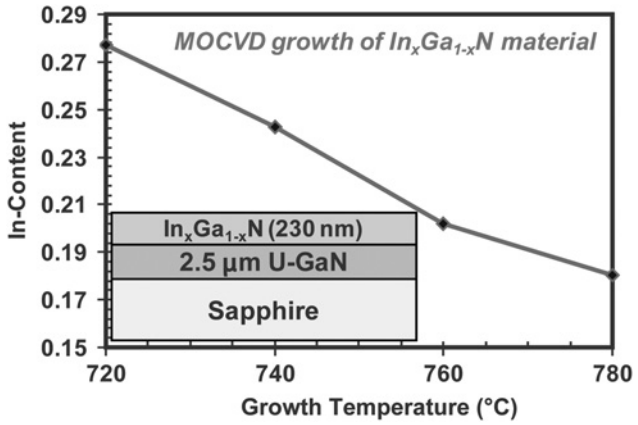

Figure 9 *Calibration studies of the In-contents in $In_xGa_{1-x}N$ layer grown by MOCVD, as a function of growth temperature*

calibration of In-contents of InGaN alloy grown at various growth temperatures were obtained by X-ray diffraction (XRD) measurements. From our studies, we found that the In-content decreases following a relatively linear relation with increasing growth temperature. The In-content in InGaN layer decreases from 28% to 18% as the growth temperature increases from 720°C to 780°C. By employing the grading in growth temperature, the compositional engineering of the In-contents in the InGaN QW can be achieved.

8 Characterisations of staggered InGaN QW LEDs

The device performance characteristics of the three-layer staggered InGaN QW LEDs are compared to those of the conventional InGaN QW. To evaluate the three-layer staggered InGaN QW grown by temperature-graded profile as active region for LEDs, both conventional and three-layer staggered InGaN LEDs were grown and fabricated. Both conventional and three-layer staggered InGaN QW were grown by MOCVD on 2.5 μm thick n-doped GaN ($T_g \sim 1075$°C) grown on *c*-plane double-side polished sapphire substrate, employing a low-temperature 30-nm GaN buffer layer ($T_g \sim 515$°C). The conventional QW structure consists of four-period 3.5-nm thick $In_{0.24}Ga_{0.76}N$ QWs, which was grown at 740°C with growth time $t = 1.09$ min. The In-content in conventional InGaN QW is calibrated as 24%. The staggered InGaN QW LEDs consists of four periods of the three-layer staggered InGaN QW. The three-layer staggered InGaN QW consists three InGaN layers with the higher In-content InGaN layer (layer #2, $T_2 = 725$°C) in the centre sandwiched between two lower In-content InGaN layers (layers #1 and #3, $T_1 = 755$°C). The growth time for the layer #1, layer #2 and layer #3 are $t_1 = 0.25$ min, $t_2 = 0.29$ min and $t_3 = 0.25$ min, respectively, with the ramping-up and ramping-down time $t_p = 0.15$ min. From our calibration studies, we estimated the In-contents in the three-layer staggered InGaN QW are 21%, 28% and 21%, with the estimated thicknesses from calibration as 1.05, 1.4 and 1.05 nm, respectively. Both the conventional InGaN QW and three-layer staggered InGaN QW were designed for achieving similar peak emission wavelength in LED operation, with nominal similar total QW thickness. We employed 10-nm u-GaN barrier layer between QW active regions in all the device structures studied. On top of the top barrier layer, 200-nm thick p-type GaN with Mg doping of 3×10^{17} cm^{-3} were grown. The LED devices were fabricated for both samples, and Ti/Au as n-contact and Ni/Au as p-contact were evaporated followed by contact annealing.

The luminescence characteristics of both the conventional and three-layer staggered InGaN QW samples were studied by power-density-dependent CL measurements. For these CL measurements performed at room temperature, we

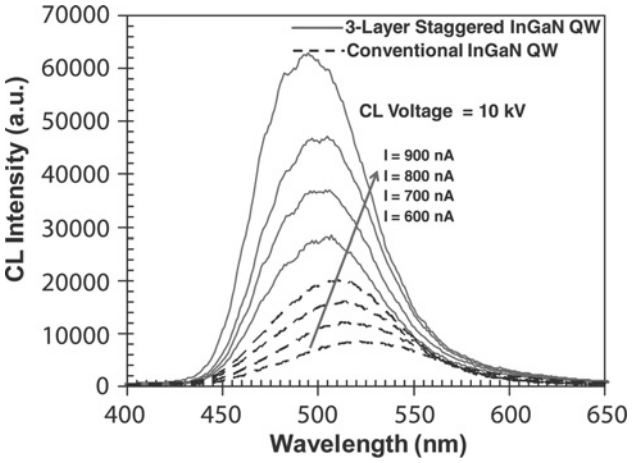

Figure 10 *CL spectra of conventional and three-layer staggered InGaN QWs emitting at 520 nm with various pumping current from I = 600 nA up to I = 900 nA at T = 300 K*

utilised a 10 keV electron beam in spot mode (area size of 1.965×10^{-9} cm^2). The high electron beam accelerating energy of 10 keV was utilised to penetrate through the 200 nm thick p-GaN layer, which was grown on top of the InGaN QW active region. To study the effect of the pumping power on the CL intensity for both the conventional and three-layer staggered InGaN QW LED structures, different excitation power density levels were applied on both of the conventional and three-layer staggered InGaN QW LED samples. The various excitation power densities were obtained by varying the electron beam current (with constant accelerating voltage of 10 keV) from 20 nA up to 950 nA.

Fig. 10 shows the measured CL spectra plotted against pumping current (shown for 600, 700, 800 and 900 nA) of the conventional and three-layer staggered InGaN QW. The staggered InGaN QW sample exhibited improved peak luminescence by up to ~3 times that of the conventional QW. Note that the peak emission wavelengths of both the conventional and staggered InGaN QWs show blue shift from 525 to 500 nm when the pumping current increases, which is due to the carrier screening effect.

Integrated CL intensities for both conventional and three-layer staggered InGaN QW samples were obtained by integration of the spectral data and are plotted against the current from 20 nA up to 950 nA, as shown in Fig. 11. The integrated CL intensity of the three-layer staggered InGaN QW exhibits improvement by 1.8–2.8 times compared to the conventional QW.

Fig. 12 shows the electrical luminescence (EL) for the conventional InGaN QWs LED and three-layer staggered InGaN QWs LED emitting at 520–525 nm, measured under continuous wave (CW) operation at room

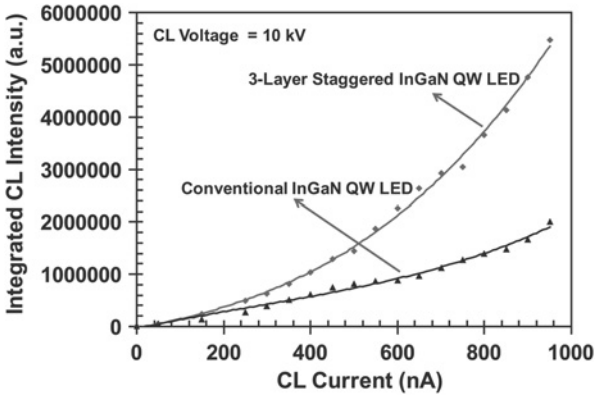

Figure 11 *EL output power against current density for conventional InGaN QW and three-layer staggered InGaN QW LEDs with λ_{peak} = 500–525 nm*

temperature. Both devices were based on bottom-emitting square device, with area size of 510 μm × 510 μm. The enhancement of the peak EL for the three-layer staggered InGaN LED as compared to the conventional LED is 1.8 times (1.3 times) at $I = 100$ mA ($I = 200$ mA). Note that the full width at half maximum (FWHM) for the EL spectra of the three-layer staggered InGaN LED is wider, in comparison to that of the conventional InGaN LED, in particular for high injection current level. This broadening could potentially result from the less abrupt interfaces in the three-layer staggered InGaN QW, or the increased inhomogeneous broadening in the higher In-content InGaN layer.

Fig. 13 shows the output power against the inject current density for conventional and three-layer staggered InGaN LEDs. The output power of the three-layer staggered InGaN QW LED was measured as 2.0–3.5 times higher in comparison to that measured from conventional InGaN QW LED, as a result from the higher intensity and broadened FWHM of the spectra from staggered QW.

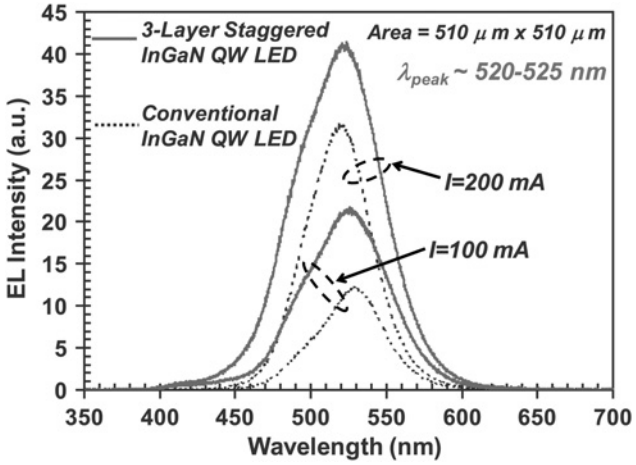

Figure 12 *EL spectra for conventional InGaN QW and three-layer staggered InGaN QW LEDs emitting with peak wavelengths at 520–525 nm*

doi: 10.1049/iet-opt.2009.0050

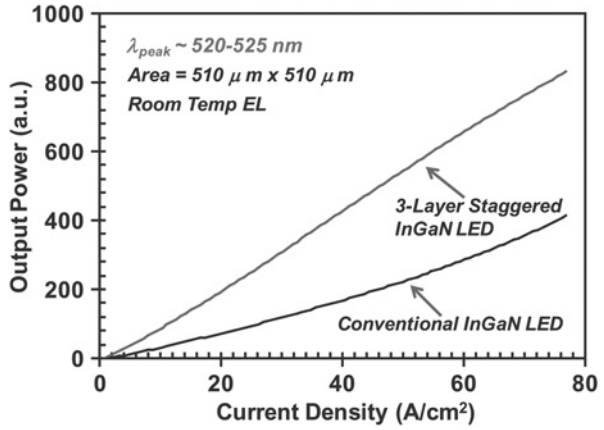

Figure 13 *Light output power against current density for conventional InGaN QW and three-layer staggered InGaN QW LEDs*

The enhancement observed in both radiative efficiency and output power of the CW EL measurements for three-layer staggered InGaN QW LEDs are in good agreement with the predicted theory.

The time-resolved photoluminescence (TR-PL) measurements were performed for both conventional and three-layer staggered InGaN QW LED samples emitting at 520–525 nm, as shown in Fig. 14. The TR-PL measurements were carried out by utilising the Nd:YAG laser amplifier with tuneable wavelength from 200 nm up to 10 μm. The excitation laser wavelength employed for the measurements of the InGaN QWs samples was 430-nm with pulse duration and repetition rate of 25 ps and 10 Hz, respectively. The output power for the excitation laser beam was 30 μJ with the diameter of the laser beam of ~80 μm. Thus, the PL excitation employed in the TR-PL measurement was about 0.6 W/cm^2. The photomultiplier tube (Thermo Oriel Instruments 70705) was used as the detector for the emission from the InGaN QW LEDs samples. The Lecroy LT584 oscilloscope with 1 GHz bandwidth was used to collect and display the time evolution of PL intensity signals from the TR-PL measurements. From the TR-PL measurements on LED device sample (shown in Fig. 14), the three-layer staggered InGaN QW exhibited 35% reduction of carrier lifetime ($\tau_{\_staggered} = 12.3$ ns), in comparison to that ($\tau_{\_conventional} = 18.9$ ns) of conventional InGaN QW. The TR-PL measurements were also conducted on PL samples (with no p-GaN cap layer), and the measurements also indicated 35–40% reduction of the carrier lifetime observed for three-layer staggered InGaN QW in comparison to those measured of conventional InGaN QW PL samples. The enhancement in both radiative efficiency and output power of the three-layer staggered InGaN QW LEDs, accompanied by a reduction in carrier lifetime, indicated that the increase in radiative recombination rate from the improved electron–hole wavefunction overlap as a dominant contributing factor to the improved device characteristics.

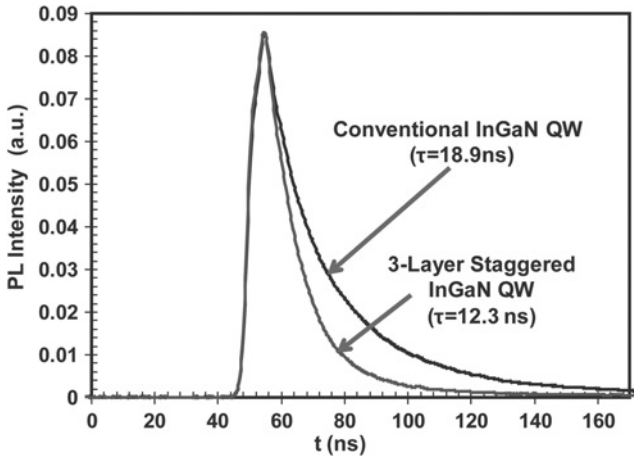

Figure 14 *Time-resolved measurements on both three-layer staggered InGaN QW and conventional InGaN QW LED samples, with peak emission wavelength at 520–525 nm*

The measurements were carried out by employing 430-nm excitation lasers with pulse duration of 25 ps

9 Summary

In summary, staggered InGaN QW as active region for LEDs emitting at 520–525 nm was investigated both numerically and experimentally. Comprehensive design studies were carried out by employing self-consistent six-band ***k·p*** method, taking into account valence band mixing, strain effect, spontaneous and piezoelectric polarisations as well as the carrier screening effect. Both two-layer and three-layer staggered InGaN QW structures with optimised In-content and sub-layer QW thickness show significantly improved radiative recombination rate and radiative efficiency as compared to that of the conventional InGaN QW emitting at 520–525 nm.

Three-layer staggered InGaN QWs grown by MOCVD employing graded temperature profile were demonstrated as improved active region for III-nitride LED emitting at 520–525 nm. The power-dependent CL measurement indicates 1.8–2.8 times enhancement for the three-layer staggered InGaN QW. The radiative efficiency of three-layer staggered InGaN QW LED is improved by 2.0–3.5 times, in comparison to that of the conventional InGaN QW. Based on the improvement in the radiative efficiency of three-layer staggered InGaN QW LED, the improved device characteristics of three-layer staggered InGaN QW can be attributed to the increase in the radiative recombination rate of the novel QW active region in agreement with theory. TR-PL measurements also indicated 35% carrier lifetime reduction in three-layer staggered InGaN QW. The increase in output power and radiative efficiency of staggered InGaN QW LEDs, accompanied by a reduction in carrier lifetime, provided good indication that the radiative recombination rate in staggered InGaN QW was enhanced. Although the current

studies focused on the optimisation of LED active region, the staggered InGaN QW active region has the potential for achieving high optical gain for laser applications. Future work on the optimisation and understanding of efficiency-droop for staggered InGaN QWs is important, in particular, for staggered InGaN QW with larger In-content difference between the inner- and outer layers.

10 Acknowledgments

The authors would like to acknowledge funding from US Department of Energy (#DE-FC26-08NT01581) and US National Science Foundation (ECCS-0701421) for the supports of these works.

11 References

[1] NAKAMURA S., SENOH M., IWASA N., NAGAHAMA S., YAMADA T., MUKAI T.: 'Superbright green InGaN single-quantum-well-structure light-emitting diodes', *Jpn. J. Appl. Phys.*, 1995, **2**, (34), pp. L1332–L1335

[2] ZHANG J., YANG J., SIMIN G., *ET AL.*: 'Enhanced luminescence in InGaN multiple quantum wells with quaternary AlInGaN barriers', *Appl. Phys. Lett.*, 2000, **77**, (17), pp. 2668–2670

[3] GUO X., LI Y.L., SCHUBERT E.F.: 'Efficiency of GaN/InGaN light-emitting diodes with interdigitated mesa geometry', *Appl. Phys. Lett.*, 2001, **79**, (13), pp. 1936–1938

[4] BROWN I.H., BLOOD P., SMOWTON P.M., *ET AL.*: 'Time evolution of the screening of piezoelectric fields in InGaN quantum wells', *IEEE J. Quantum Electron.*, 2006, **42**, (12), pp. 1202–1208

[5] EE Y.K., KUMNORKAEW P., ARIF R.A., *ET AL.*: 'Optimization of light extraction efficiency of III-nitride light emitting diodes with self-assembled colloidal-based microlenses', *IEEE J. Sel. Top. Quantum Electron.*, 2009, **15**, (4), pp. 1218–1225

[6] KRAMES M.R., OCHIAI-HOLCOMB M., HÖFLER G.E., *ET AL.*: 'High-power truncated-inverted-pyramid $(Al_xG_{a1-x})_{0.5}I_{n0.5}P/GaP$ light-emitting diodes exhibiting >50% external quantum efficiency', *Appl. Phys. Lett.*, 1999, **75**, (16), pp. 2365–2367

[7] KRAMES M.R., SHCHEKIN O.B., MUELLER-MACH R., *ET AL.*: 'Status and future of high-power light-emitting diodes for solid-state lighting', *J. Display Technol.*, 2007, **3**, (2), pp. 160–175

[8] FARRELL R.M., FEEZELL D.F., SCHMIDT M.C., *ET AL.*: 'Continuous-wave operation of AlGaN-cladding-free nonpolar *m*-plane InGaN/GaN laser diodes', *Jpn. J. Appl. Phys.*, 2007, **46**, (32), pp. L761–L763

[9] PARK J., KAWAKAMI Y.: 'Photoluminescence property of InGaN single quantum well with embedded AlGaN δ layer', *Appl. Phys. Lett.*, 2006, **88**, (20), p. 202107

[10] PARK S.H., PARK J., YOON E.: 'Optical gain in InGaN/GaN quantum well structures with embedded AlGaN delta layer', *Appl. Phys. Lett.*, 2007, **90**, (2), p. 023508

[11] ARIF R.A., EE Y.K., TANSU N.: 'Polarization engineering via staggered InGaN quantum wells for radiative efficiency enhancement of light emitting diodes', *Appl. Phys. Lett.*, 2007, **91**, (9), p. 091110

[12] ARIF R.A., ZHAO H., EE Y.K., TANSU N.: 'Spontaneous emission and characteristics of staggered InGaN quantum-well light-emitting diodes', *IEEE J. Quantum Electron.*, 2008, **44**, (6), pp. 573–580

[13] ZHAO H., ARIF R.A., TANSU N.: 'Design analysis of staggered InGaN quantum wells light-emitting diodes at 500–540 nm', *IEEE J. Sel. Top. Quantum Electron.*, 2009, **15**, (4), pp. 1104–1114

[14] ZHAO H., LIU G., LI X.H., *ET AL.*: 'Growths of staggered InGaN quantum wells light-emitting diodes emitting at 520–525 nm employing graded growth-temperature profile', *Appl. Phys. Lett.*, 2009, **95**, (6), p. 061104

[15] PARK S.H., AHN D., KIM J.W.: 'High-efficiency staggered 530 nm InGaN/InGaN/GaN quantum-well light-emitting diodes', *Appl. Phys. Lett.*, 2009, **94**, (4), p. 041109

[16] PARK S.H., AHN D., KOO B.H., KIM J.W.: 'Electronic and optical properties of staggered InGaN/InGaN quantum-well light-emitting diodes', *Phys. Stat. Sol. A*, 2009, **206**, (11), pp. 2637–2640

[17] ARIF R.A., ZHAO H., TANSU N.: 'Type-II InGaN–GaNAs quantum wells active regions for lasers applications', *Appl. Phys. Lett.*, 2008, **92**, (1), p. 011104

[18] ZHAO H., ARIF R.A., TANSU N.: 'Self consistent analysis of Type-II 'W' InGaN–GaNAs quantum well lasers', *J. Appl. Phys.*, 2008, **104**, (5), p. 043104

[19] ZHAO H., ARIF R.A., EE Y.K., TANSU N.: 'Optical gain analysis of strain-compensated InGaN–AlGaN quantum well active regions for lasers emitting at 420–500 nm', *Opt. Quantum Electron.*, 2008, **40**, (5–6), pp. 301–306

[20] ZHAO H., ARIF R.A., EE Y.K., TANSU N.: 'Self-consistent analysis of strain-compensated InGaN–AlGaN quantum wells for lasers and light-emitting diodes', *IEEE J. Quantum Electron*, 2009, **45**, (1), pp. 66–78

[21] CHUANG S.L., CHANG C.S.: 'A band-structure model of strained quantum-well wurtzite semiconductors', *Semicond. Sci. Technol.*, 1997, **12**, (3), pp. 252–263

doi: 10.1049/iet-opt.2009.0050

[22] CHUANG S.L., CHANG C.S.: '$k \bullet p$ method for strained wurtzite semiconductors', *Phys. Rev. B.*, 1996, **54**, (4), pp. 2491–2504

[23] CHUANG S.L.: 'Physics of optoelectronics devices' (Wiley, New York, 1995), ch. 4 and 9

[24] VURGAFTMAN I., MEYER J.R.: 'Electron bandstructure parameters', in PIPREK J. (ED.): 'Nitride semiconductor devices', ch. 2

[25] VURGAFTMAN I., MEYER J.R.: 'Band parameters for nitrogen-containing semiconductors', *J. Appl. Phys.*, 2003, **94**, (6), pp. 3675–3696

[26] VAN DE WALLE C.G., NEUGEBAUER J.: 'Small valence-band offsets at GaN/InGaN heterojunctions', *Appl. Phys. Lett.*, 1997, **70**, (19), pp. 2577–2579

[27] CHUANG S.L.: 'Optical gain of strained wurtzite GaN quantum-well lasers', *IEEE J. Quantum Electron.*, 1996, **32**, (10), pp. 1791–1800

[28] HADER J., MOLONEY J.V., PASENOW B., *ETAL.*: 'On the importance of radiative and Auger losses in GaN-based quantum wells', *Appl. Phys. Lett.*, 2008, **92**, (26), p. 261103

[29] HADER J., MOLONEY J.V., THRANHARDT A., KOCH S.W.: 'Interband transitions in InGaN quantum wells', in PIPREK J. (ED.): 'Nitride semiconductor devices', ch. 7

[30] SHEN Y.C., MUELLER G.O., WATANABE S., GARDNER N.F., MUNKHOLM A., KRAMES M.R.: 'Auger recombination in InGaN measured by photoluminescence', *Appl. Phys. Lett.*, 2007, **91**, (14), p. 141101

[31] SCHUBERT M.F., CHHAJED S., KIM J.K., *ET AL.*: 'Effect of dislocation density on efficiency droop in GaInN/GaN light-emitting diodes', *Appl. Phys. Lett.*, 2007, **91**, (23), p. 231114

[32] SON J.K., LEE S.N., PAEK H.S., *ET AL.*: 'Radiative and non-radiative transitions in blue quantum wells embedded in AlInGaN-based laser diodes', *Phys. Stat. Sol. (c)*, 2007, **4**, (7), pp. 2780–2783

[33] SCHWARZ Y., BRAUN H., KOJIMA K., KAWAKAMI Y., NAGAHAMA S., MUKAI T.: 'Interplay of built-in potential and piezoelectric field on carrier recombination in green light emitting InGaN quantum wells', *Appl. Phys. Lett.*, 2007, **91**, (12), p. 123503

[34] TANSU N., MAWST L.J.: 'Current injection efficiency of 1300-nm InGaAsN quantum-well lasers', *J. Appl. Phys.*, 2005, **97**, (5), p. 054502

[35] PARK S.H., CHUANG S.L.: 'Many-body optical gain of wurtzite GaN-based quantum-well lasers and comparison with experiment', *Appl. Phys. Lett.*, 1998, **72**, (3), pp. 287–289